JOURNAL OF THE CANADIAN SOCIETY OF EXPLORATION GEOPHYSICISTS
VOL 23, NO 1 (DEC 1987), P. 56-65

LINEARIZED INVERSION OF SEISMIC AMPLITUDE DATA[1]

M. SHAHRIAR[2], F. HRON[2] AND G.L. CUMMING[2]

ABSTRACT

An efficient technique for the linearized inversion of seismic amplitude data is presented. Parameterization of the forward problem is developed using Asymptotic Ray Theory (ART). It is demonstrated that simultaneous use of both kinematic and dynamic data results in a better resolution of the model parameters and reveals additional information such as density and shear-wave velocities along with the usual compressional-wave velocity computations. The program has been tested for multiple-layered and horizontally structured Earth models using head waves and primary and multiple reflections including low-velocity zones and multiple shotpoints. Excellent numerical results for relatively simple models indicate the possibility of further application of the method for more realistic and complex geological structures.

INTRODUCTION

Linearized inversion for nonlinear problems has been used by many geophysicists (Braile, 1973; Vignersesse, 1978; Hoversten *et al.*, 1982) for over a decade now. In seismology most of the studies involve inversion of traveltime data (*i.e.*, kinematic information) in terms of various simple as well as complex Earth models (Aki and Lee, 1976; Crosson, 1976; Benz and Smith, 1984; Hirahara and Ishikawa, 1984; Ivansson, 1985; Ursin and Zheng, 1985; Chiu *et al.*, 1986). It is a well established fact that the inversion of seismic data remains incomplete without involving the dynamic information (*i.e.*, amplitude) available in the data. Most often, use of amplitude information has been carried out in terms of visual waveform matching using synthetic seismograms. Very few attempts have been made to use this technique for the direct inversion of quantitative amplitude data. This is partly because of the complexity involved in suitable parameterization of the amplitude function in terms of Earth structure and also to a considerable extent because of enormous computer time involved in the repeated forward ray-tracing calculations.

In this paper we present an efficient technique for the parameterization and inversion of amplitude data using Asymptotic Ray Theory (ART), and the least-squares method. The analysis yields Earth structure in terms of density, compressional- and shear-wave velocities for isotropic, homogeneous and horizontally layered models. The program has been used for both head-wave and reflection amplitudes including multiple reflection arrivals. Excellent numerical results indicate the potential of this method for further application in complex geological structures.

Computation of the response at specific geophone locations has been accomplished using a two-point ray-tracing algorithm. All the calculations have been performed using both analytical and numerical approaches for comparison. It has been found that the analytical computations are more accurate (as expected) and involve less computation time. A few iterations (typically 3 to 6 iterations) have been enough to get an acceptable fit in terms of a root-mean-squared (rms) deviation criterion.

One advantage of the technique is that both kinematic and dynamic information may be used simultaneously without data modification. It has been found that combined use of both types of data results in a better resolution of the model parameters. Moreover, since density and P- and S-wave velocities are computed simultaneously, a quantitative estimation of the elastic properties of the medium under study is also possible using this method. The program can be used for multiple layers and multiple shotpoints. Converted phases may be incorporated easily with only slight modifications. This method is also successful in detecting low-velocity zones and multiple arrivals which always have been a difficult problem for kinematic inversion methods.

The most important drawback of this method is that it cannot be applied for the amplitudes near the critical region, especially with low-frequency signals. This is due to the fact that the plane-wave reflection coefficient

[1]Presented at the C.S.E.G. National Convention, Calgary, Alberta, May 15, 1986. Manuscript received by the Editor October 14, 1986; revised manuscript received July 29, 1987.

[2]Institute of Earth and Planetary Physics, Department of Physics, University of Alberta, Edmonton, Alberta T6G 2J1

which is used for the amplitude computation in ART exhibits an infinite derivative in the vicinity of the critical angle. This drawback can be overcome if a suitable high-frequency approximation in terms of the Weber function is used (Marks and Hron, 1979).

The program has been designed for numerical modelling as well as interpretation of field amplitude data. Conventional seismic records often fail to represent the true amplitudes due to lack of proper control over the geophone gains and also because of variations in the geophone-to-ground coupling. Therefore, for the present, the program has been applied to synthetic data only.

The Inverse Method

Geophysical inversion (Aki and Richards, 1980; Lines and Treitel, 1984) may be considered as a process of fitting a finite set of observed data to the response of an idealized Earth model. The model usually consists of a set of mathematical relations representing the physical process involved. These equations contain a finite number of independent variables (*e.g.*, velocity, density, thickness, etc.) called the model parameters **X**. The model response **f** may be a linear or nonlinear function of the model parameters. For the nonlinear case it is usually possible to approximate a quasi-linear system by using a first-order Taylor series expansion of the final response **f** about some arbitrary starting response $\mathbf{f}^0$,

$$f_i = f_i^0 + \sum_{j=1}^{n} \left.\frac{\partial f_i}{\partial X_j}\right|_x^0 \left(X_j - X_j^0\right) \tag{1}$$

where f_i = final model response at ith observation point,
f_i^0 = initial response at ith observation point,
X_j = final value of jth model parameter,
X_j^0 = initial estimate of jth model parameter,
n = total number of model variables.

For m number of observation points, equation (1) constructs an array of numbers which can be expressed in matrix form as

$$|\mathbf{A}|\,|\Delta\mathbf{X}| = |\Delta\mathbf{B}| \tag{2}$$

where $A_{ij} = \partial f_i/\partial X_j \,|_x^0$
$\Delta\mathbf{X} = \mathbf{X} - \mathbf{X}^0$
$\Delta\mathbf{B} = \mathbf{f} - \mathbf{f}^0$
$i = 1,2 \ldots .m; j = 1,2, \ldots .n.$

Calculation of the derivatives A_{ij} may be performed analytically or numerically. Analytical calculations are preferred for speed and accuracy. The residual vector $\Delta\mathbf{B}$ contains the difference between the observed and initially computed amplitudes. It is clear from (2) that the correction vector $\Delta\mathbf{X}$ can be obtained from

$$|\Delta\mathbf{X}| = |\mathbf{A}|^{-1}\,|\Delta\mathbf{B}| \tag{3}$$

so that final improved vector is

$$|\mathbf{X}| = |\mathbf{X}^0| + |\mathbf{A}|^{-1}\,|\Delta\mathbf{B}|\,. \tag{4}$$

If $\mathbf{X}^0$ differs from **X** significantly, it may be necessary to iterate towards **X** until $\Delta\mathbf{B}$ is small. The above linearization process does not change the nonlinear behavior of the problem. If an initial estimate of the solution close to the exact one is available, the above linear equations may be safely applied to a localized quasi-linear zone close to the exact solution. Convergence attempts are restricted to this localized zone only. Geophysical inverse problems may however possess several localized linear zones resulting in a nonuniqueness problem. To isolate the best solution from several possible ones, the seismologist has to apply his or her own instinct or bias, developed from previous knowledge of the approximate solution obtained from other studies conducted in the same area.

In equation (3), the exact inverse $\mathbf{A}^{-1}$ exists only if **A** is a square matrix. For most geophysical problems there are more observations than model parameters making **A** a rectangular matrix. Therefore, if a solution exists, it should be determined by a least-squares method. Let the error for each data set be **E**:

$$|\mathbf{E}| = |\mathbf{A}|\,|\Delta\mathbf{X}| - |\Delta\mathbf{B}| \tag{5}$$

Minimization of the squared norm $\mathbf{E}^t\mathbf{E}$ (^{t} means transpose) with respect to the solution vector $\Delta\mathbf{X}$ leads to a set of normal equations of the form

$$|\Delta\mathbf{X}| = |\mathbf{A}^t\mathbf{A}|^{-1}\,|\mathbf{A}^t\Delta\mathbf{B}| \tag{6}$$

A more convenient form of the solution may be obtained by using the Singular Value Decomposition (SVD) (Lanczos, 1961; Golub and Reinsch, 1970; Lines and Treitel, 1984) in which

$$|\mathbf{A}| = |\mathbf{U}|\,|\Lambda|\,|\mathbf{V}|^t \tag{7}$$

where **U** and **V** are semiorthogonal matrices whose columns are respectively the basis vectors spanning the region of the data space and the solution space activated by the operator **A**. Λ is the diagonal matrix having the eigenvalues of **A**. A suitable inverse operator $\mathbf{A}^{-1}$ is then given by

$$|\mathbf{A}|^{-1} = |\mathbf{V}|\,|\Lambda|^{-1}\,|\mathbf{U}|^t \tag{8}$$

which is called the natural or generalized or Lanczos inverse of **A**. The solution of the problem is calculated using equations (4) and (8). In practical applications, however, a positive small value called the damping parameter (Lines and Treitel, 1984) is added to the diagonal elements of Λ to overcome the solution instability. Methods of estimating the damping parameter have been discussed by Hoerl *et al.* (1975), Aki and Lee (1976) and Crosson (1976).

The Direct Problem

The most important part of the inversion process is to develop an efficient program to solve the direct problem. Since it is particularly important to consider a model where all the model parameters contribute effectively

and uniformly, the parameterization of the model under consideration demands special attention. ART has been used to accommodate most essential parameters in the forward problem. Zeroth- and first-order formulae (Cerveny and Ravindra, 1971) have been employed respectively for the computation of reflection and head-wave amplitudes. Assuming that seismic waves travel through the elastic medium along well defined paths, the geometrical ray approach has been adopted to calculate the geometrical spreading. For simplicity we have considered an isotropic Earth structure with plane horizontal layers and a laterally homogeneous medium.

Computation of amplitude

ART provides a time-domain solution to the elastodynamic equation and the boundary conditions in the form of an asymptotic ray series in inverse powers of frequency. Cerveny and Ravindra (1971) have used ART to derive the following expressions for the vertical components of reflected and head-wave amplitudes from a point source to the receiver, both located on the surface (Figure 1).

$$L = \frac{\cos\theta_1}{v_1}\left[\sum_{j=1}^{s}\left(\frac{h_j\, v_j}{\cos\theta_j}\right)\right]^{\frac{1}{2}}\left[\sum_{j=1}^{s}\left(\frac{h_j\, v_j}{\cos^3\theta_j}\right)\right]^{\frac{1}{2}} \quad (9)$$

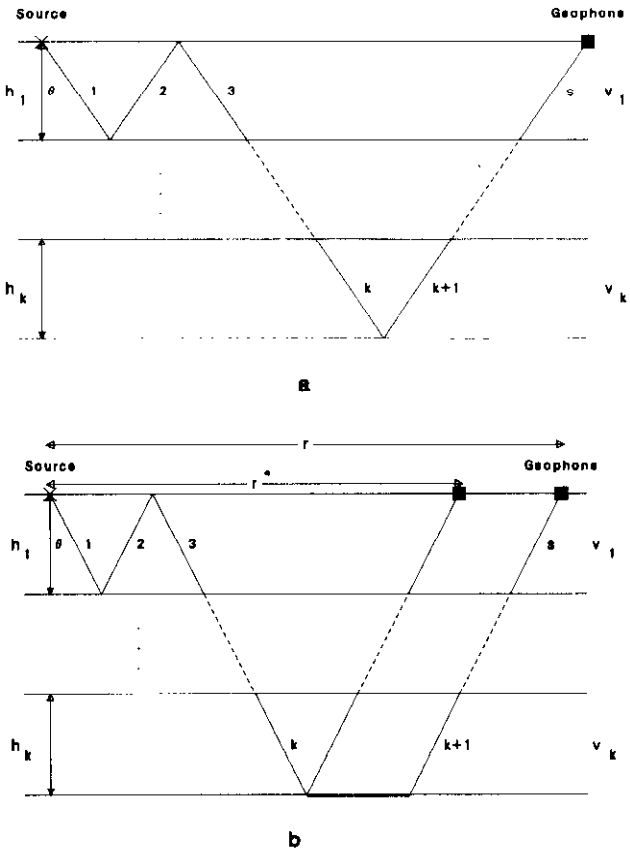

Fig. 1. Sketch showing ray segments required to compute (a) reflection and (b) head-wave amplitudes for a multilayered medium.

$$A_{refl} = \frac{\prod_{j=1}^{s}\Re_j\,\eta_z}{L} \quad (10)$$

$$A_{head} = \frac{v_1 \tan\theta_1\,\Gamma_k \prod_{\substack{j=1\\ j\neq k}}^{s}\Re_j\eta_z}{\left[\omega r^{\frac{1}{2}}\,(r-r^*)^{\frac{3}{2}}\right]} \quad (11)$$

where k = index for the critically refracted ray segment,

L = geometrical spreading,

$\Re_j$ = reflection or transmission coefficient,

Γ_k = head-wave coefficient for critical refraction,

v_j = velocity along the jth ray segment,

h_j = thickness of the layer containing the jth ray segment,

θ_j = the angle of incidence at the jth interface on which the ray impinges,

s = total number of segments in the ray,

ω = dominant source frequency

r = source-to-receiver offset distance,

r^* = critical distance,

η_z = a unit vector tangent to the last ray segment.

To calculate multiple-reflection arrivals, corresponding changes in the expression for the geometrical spreading must be made to account for the additional ray segments. The critical distance r^* is given by

$$r^* = 2\sum_{j=1}^{n} h_j v_j \left(v_n^2 - v_j^2\right)^{-\frac{1}{2}} \quad (12)$$

where n is the total number of layers. Using the same notation as Cerveny and Ravindra (1971), the PP transmission coefficient $\Re_{13}$, the PP reflection coefficient $\Re_{11}$ and the PPP head-wave coefficient Γ_{131} respectively are given by

$$\Re_{13} = \frac{2\alpha_1\rho_1 P_1\left(\beta_2 P_2 X + \beta_1 P_4 Y\right)}{D} \quad (13)$$

$$\Re_{11} = -1 + \frac{2P_1\left(\alpha_2\beta_2 P_2 X^2 + \beta_1\alpha_2\rho_1\rho_2 P_4 + q^2 p^2 P_2 P_3 P_4\right)}{D} \quad (14)$$

$$\Gamma_{131} = 2\alpha_1\alpha_2\rho_1\rho_2\left[\frac{P_1\left(\beta_2 P_2 X + \beta_1 P_4 Y\right)^2}{D^2}\right] \text{ at } p=\frac{1}{\alpha_2} \quad (15)$$

where $P_1 = (1-\alpha_1^2 p^2)^{1/2}$,

$P_2 = (1-\beta_1^2 p^2)^{1/2}$,

$P_3 = (1-\alpha_2^2 p^2)^{1/2}$,

$P_4 = (1-\beta_2^2 p^2)^{1/2}$,

$X = \rho_2 - qp^2$,

$Y = \rho_1 + qp^2$,

$Z = \rho_2 - \rho_1 - qp^2$,

$q = 2(\rho_2\beta_2^2 - \rho_1\beta_1^2)$,

$$D = \alpha_1\alpha_2\beta_1\beta_2 p^2 Z^2 + \alpha_2\beta_2 P_1 P_2 X^2 + \alpha_1\beta_1 P_3 P_4 Y^2 + \rho_1\rho_2(\alpha_2\beta_1 P_1 P_4 + \alpha_1\beta_2 P_2 P_3) + q^2 p^2 P_1 P_2 P_3 P_4,$$

p = ray parameter,

ρ_1,α_1,β_1 = density, P and S velocity in the layer containing the incident ray segment,

ρ_2,α_2,β_2 = density, P and S velocity in the layer containing the reflected or refracted ray segment.

The ray parameter p plays an auxiliary role if the amplitude at a given source-to-receiver distance is required. In this case p must be determined using a suitable numerical process (next section).

Computation of traveltime

The reflection traveltime at a receiver located at distance X_j from source point (Figure 2) is given by

$$T_j = 2\sum_{i=1}^{n} h_i v_i^{-1}\left(1 - p_j^2 v_i^2\right)^{-\frac{1}{2}} \tag{16}$$

where n is the total number of layers. The ray parameter p_j corresponding to the offset X_j is obtained from

$$X_j = 2\sum_{i=1}^{n} h_i p_j v_i\left(1 - p_j v_i^2\right)^{-\frac{1}{2}} \tag{17}$$

using a numerical algorithm such as the Gauss-Seidel method. The head-wave travel times are computed from

$$T_j = \frac{X_j}{v_n} + 2\sum_{i=1}^{n} \frac{h_i\left(v_n^2 - v_i^2\right)^{\frac{1}{2}}}{v_n v_i} \tag{18}$$

where j = 1,2,3.....n,

n = total number of layers.

Implementation of the Method

There are three main considerations involved in the parameterization part of the process. The first one is the choice of dimension for the model space. Ordinary least squares suggests a small number of parameters to avoid error magnification due to ill-conditioning of $\mathbf{A}^t\mathbf{A}$. Moreover, it also has to be less than the dimension of the data space. Otherwise, we may have to invoke a different approach (*e.g.*, underdetermined case) utilizing a different inversion algorithm.

The next important consideration is to try to choose parameters which are truly important variables and are expected to be resolved by the data. Of course, there are situations where the relative importance of variables is not well-known beforehand. In those situations, we may have to proceed with the inversion process, the variable in question being included in the parameter list, and study the corresponding resolution vector to be able to decide whether to discard the parameter.

Lastly, the parameterization should be such that it does not lead to a complicated forward model, that it is simple enough to be linearized easily and still contributes successfully toward the essential properties of the model while involving minimum computer time required for repeated forward calculations.

The total inversion process has been designed to work in two steps: (a) inversion of the kinematic data, (b) inversion of the dynamic data using results from the kinematic inversion as constraints. A flow diagram for the inversion scheme used either in step (a) or in step (b) is shown in Figure 3.

The kinematic inversion stage computes the P-wave velocities and the layer thicknesses from the traveltime data. The P velocities are then used to form the part of

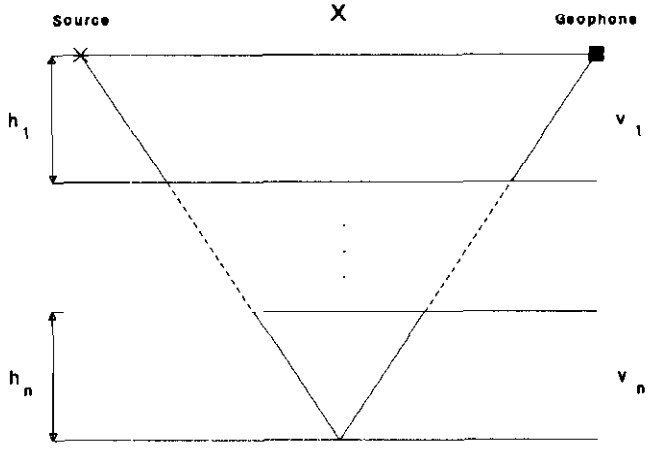

Fig. 2. Sketch showing ray segments required to compute reflection traveltimes for a multilayered medium.

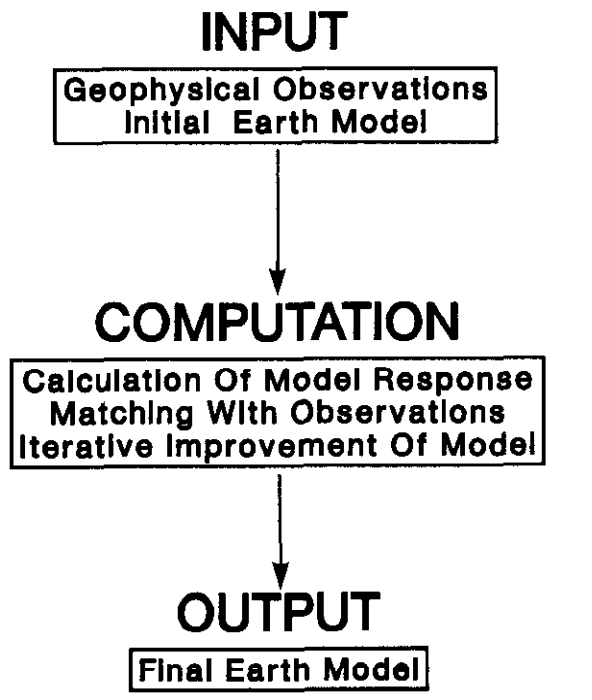

Fig. 3. Flow diagram for the inversion scheme.

the initial estimation required for the inversion of the dynamic information. Since a close initial guess is very important for convergence, use of this information from stage (a) significantly improves the convergence rate in stage (b). Kinematic inversion alone is an incomplete process, because we can not get the S-wave velocities and densities from travel times. However, if we are interested in the computation of P-wave velocities and thicknesses only, results from the partial traveltime inversion in stage (a) will be sufficient enough to fulfill our requirement. Since S-wave velocities and the densities are not available from the traveltime inversion in step (a), initial estimates of these parameters are computed from the following formulae (Birch, 1964):

$$\beta = \alpha/1.732$$
$$\rho = 0.252 + 0.3788\alpha \qquad (19)$$

where α, β and ρ, respectively, are the P and S velocities and density. Equation (19) uses the P-wave velocities obtained from the kinematic inversion to estimate the initial S velocity and densities. Two different approaches, (a) the stripping method and (b) the simultaneous full-model inversion, have been tried for the inversion scheme. In the stripping process, each layer is considered separately starting from the topmost layer. Each layer has three independent parameters, the P velocity, S velocity and density. Thickness parameters obtained from the kinematic inversion are kept constant for the rest of the inversion process. This is done intentionally to reduce the number of parameters and give more emphasis to the velocity and density values. The number of layers is indicated by the number of traveltime branches in the observed seismogram. Information from the upper layers (as computed from the partial inversion) is used to reduce the number of parameters required to compute the lower layers. In the full-model inversion, however, all the model parameters are computed simultaneously. In the latter case, the transformation matrix **A** contains the information from all the specified arrivals (*e.g.*, direct, Pg-branches and Pn-arrivals) and includes the effects of all the model parameters and the data-recording sites. It is obvious that the dimension of the matrix is much larger than in the previous case. Therefore, we have found the stripping method more convenient than the full-model inversion in terms of storage space, total processing time and convergence. For example, a typical full-model inversion required 6 iterations, whereas, using the stripping method, the same data were inverted in 3 iterations. For all the models we have tested, the final result remains the same in both cases.

Decomposition of the matrix **A** into **U**, **Λ** and **V** has been carried out using a subroutine given by Forsythe *et al.* (1977). The inversion process may be designed such that all the calculations are performed systematically without interruption, and stopping occurs at the final model automatically when required convergence criteria are met. On the other hand, it is also possible to interrupt between calculation steps to inspect the elements of **U** and **V** for the terms responsible for slow convergence. It is also interesting to monitor results at the end of each iteration before final convergence and to study the solution growth pattern. Both options ultimately lead to the same result, but in most of the cases it is convenient to use the first option. Estimation of the damping parameter may also be designed to be an automatic process (Chiu *et al.*, 1986), but we have found that the automation process is rather expensive. Instead, we have determined it after a few trial runs starting with a value of 1.0 and reducing it further in the subsequent steps. In most of the synthetic examples, the classical least squares (no damping) has been enough, enabling us to skip this part of the computation.

Since ART does not produce reliable amplitudes at the critical angle, computation of the amplitudes has been restricted to the precritical or postcritical regions only. The partial derivatives which constitute the elements of the matrix **A** have been computed using both analytical expressions and numerical methods employing the central difference formula:

$$\partial F_i/\partial X_j \simeq [F_i(X_j+\Delta X_j) - F_i(X_j-\Delta X_j)]/2\Delta X_j \qquad (20)$$

Computation of the response at specific geophone locations has been performed using a two-point ray tracer. The ray tracer computes the ray parameter corresponding to a specific shot-receiver pair using a numerical approach. Once the ray parameter is known, the angles of incidence at each interface may be computed from the Snell's law as follows:

$$\theta_j = \sin^{-1}(v_j p) \qquad (21)$$

where p is the ray parameter and v_j is the velocity of the jth layer. Computation of amplitude is then straightforward using equations (9), (10) and (11). Results from both numerical and analytical methods have been used to compare the relative efficiency of the two methods under different conditions such as low- and high-frequency signals, small and large offset distances and thin- and thick-layered structures.

Since the amplitude values computed by the forward model are usually very small, scaling by a large multiplier may be required to ensure the necessary significant digits.

Numerical Results

Before attempting to invert real field data, it is worthwhile to investigate the reliability of the inversion program developed. A series of numerical tests have been performed in this regard. The results obtained from these tests provide some insight into the capability of the program, the effects of inherent uncertainty in the data, the error limits to the computed parameters and, above all, the reliability of the results produced by the program. The following examples include sample inversions of amplitude data from the bottom interfaces of multilayered models. It is assumed that the inversion of

traveltime branches and amplitude data from upper interfaces has been completed as the preliminary part of the stripping process. The final results include those obtained from partial inversions of (a) traveltime, (b) amplitude from upper layers and (c) amplitude from the bottom interface.

Synthetic amplitude data (Figure 4) for reflected arrivals from the bottom interface of a 3-layer velocity model (shown as exact model in Figure 5) have been generated by direct calculations using equations (9) and (10). Only data from the lower interface are displayed in Figure 4. Treating these amplitudes as the observation data, we have used the iterative inversion algorithm to calculate the final model. As expected, the final inverted model is an exact reproduction of the theoretical model (Figure 5). Convergence to the final model occurred after 3 iterations. Absolute residues have been minimized up to the order of 10^{-5}. Table 1 shows the computed model parameters along with the corresponding standard deviations and resolution values. These numbers from Table 1 imply a 100% reliable model within the specific error criteria. Overall, rms error for this inversion turns out to be 0.00002 after just three iterations. The resolution matrix indicates a high degree of uniqueness with every diagonal element showing a maximum value of 1.0.

Next we contaminated the same data randomly with a spread of maximum 10% for the traveltime data (not shown) and 5% for the amplitude data (only data from lower interface shown in Figure 6). Moreover, since in reality not all the geophones record every event, we randomly deleted some of the stations to simulate this situation. We have found that the lack of observation and contamination of the data both affect the resolution and convergence rate adversely. Moreover, there is always a maximum limit of the contamination (or noise) in the data which the program is able to tolerate for producing a model sufficiently close to the exact one. We have found that a maximum of 10% contamination to the data is allowable to get an acceptable estimate of the solution, provided the initial model is a close guess to the actual model. The results from the inversion of contaminated data is included in Table 2 and the final model is shown in Figure 7. The overall rms value is 1.0. It is also evident that the parameters for the inverted model now show larger standard deviations than the ones obtained with exact data. However, if the estimated model parameters are judged along with the estimated deviations, the agreement is still very good. Therefore, we may conclude that the program will work for both exact and noisy (within the above limits) data by carefully detecting the noise level (absolute residues

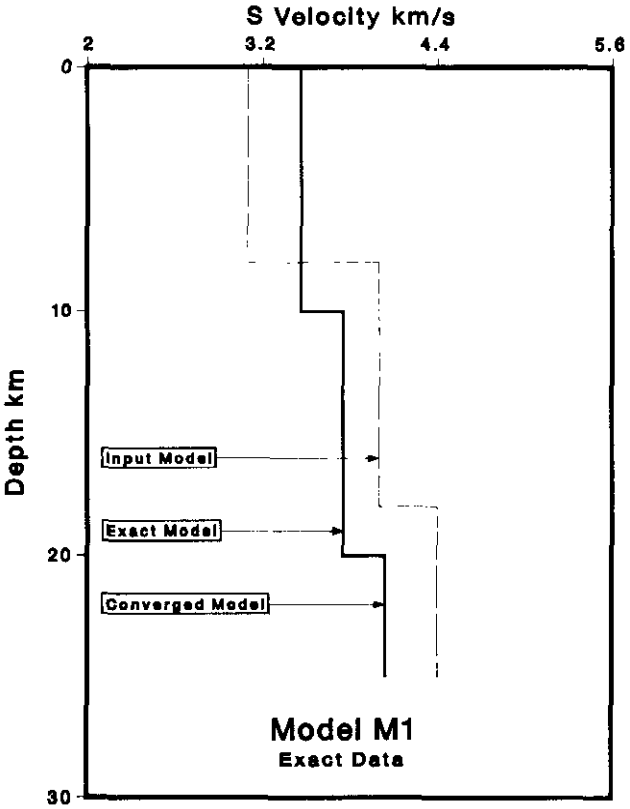

Fig. 5. Inverted velocity model M1 from noise-free amplitude data shown in Figure 4.

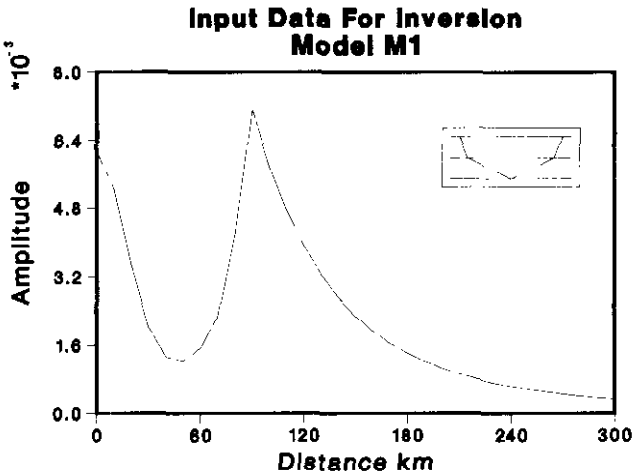

Fig. 4. Noise-free synthetic amplitude data obtained from forward calculation of model M1 shown in Figure 5.

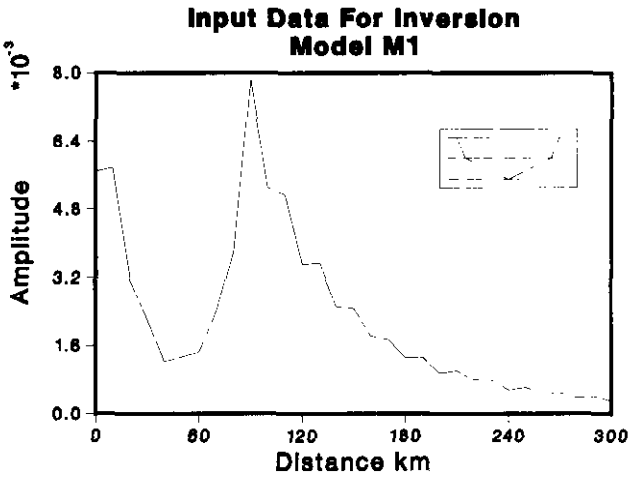

Fig. 6. Noisy synthetic amplitude data for model M1.

left at the end of inversion), by giving a quantitative estimate of the uncertainty (standard deviation) of the computed values and by indicating the reliability (resolution) of the results produced.

Layer	Exact model	Inverted Model	Resolution (diagonal)	Standard Deviation
	P-Velocity km/s			
1	6.0	6.000	1.00	.00001
2	6.5	6.500	1.00	.00001
3	7.0	7.000	1.00	.00002
	S-Velocity km/s			
1	3.464	3.464	1.00	.00001
2	3.753	3.753	1.00	.00002
3	4.042	4.042	1.00	.00002
	Density gm/cc			
1	2.525	2.525	1.00	.00001
2	2.714	2.714	1.00	.00003
3	2.904	2.904	1.00	.00003

Table 1. Results from iterative inversion of exact amplitude data for a 3-layer model.

Layer	Exact model	Inverted Model	Resolution (diagonal)	Standard Deviation
	P-Velocity km/s			
1	6.0	6.036	1.00	.04631
2	6.5	6.550	1.00	.05752
3	7.0	7.045	1.00	.05241
	S-Velocity km/s			
1	3.464	3.500	1.00	.05250
2	3.753	3.807	1.00	.06120
3	4.042	3.993	1.00	.05701
	Density gm/cc			
1	2.525	2.531	1.00	.03190
2	2.714	2.742	1.00	.02912
3	2.904	2.856	1.00	.04232

Table 2. Results from iterative inversion of contaminated amplitude data for a 3-layer model.

Layer	Exact model	Inverted Model	Resolution (diagonal)	Standard Deviation
	P-Velocity km/s			
1	6.5	6.458	1.00	.06640
2	6.0	5.963	1.00	.04755
3	7.0	6.941	1.00	.07160
	S-Velocity km/s			
1	3.753	3.700	1.00	.05139
2	3.464	3.420	1.00	.06252
3	4.042	3.950	1.00	.09170
	Density gm/cc			
1	2.714	2.679	1.00	.04142
2	2.525	2.496	1.00	.05350
3	2.904	2.944	1.00	.08366

Table 3. Results from iterative inversion of amplitude data for a 3-layer low-velocity model.

We have also tried different starting models and found that the final solution usually does not depend on the initial model. The convergence rate, however, generally depends on the choice of the initial model (examples are given in Shahriar *et al.*, 1987).

The next example we have attempted is the amplitude data (Figure 8) generated from the bottom interface of a 3-layer model with low-velocity zone in the middle crust. From the results of the inversion (shown in Table 3 and Figure 9), it is clear that the program has no difficulty detecting such anomalies in the crust provided the starting model contains an approximation to the velocity inversion.

Another example we have considered is the multiple-reflection arrivals from the second layer in a three-layer model. (The program, however, can treat multiples from any interface of a multiple-layer model.) From the visual inspection of the field seismogram alone, it is particularly troublesome to decide whether a primary- or a multiple-reflection arrival is being observed. Sometimes, these multiples may be attenuated during the common-depth-point (CDP) processing, but, unfortunately, differences in the normal moveout (NMO) are not usually large enough to identify the multiples with certainty. For long-range profiles, such as in the case of wide-angle data, it is particularly difficult to detect such arrivals. Multiples may be identified by considering the energy of the signals, but, again, a visual inspection

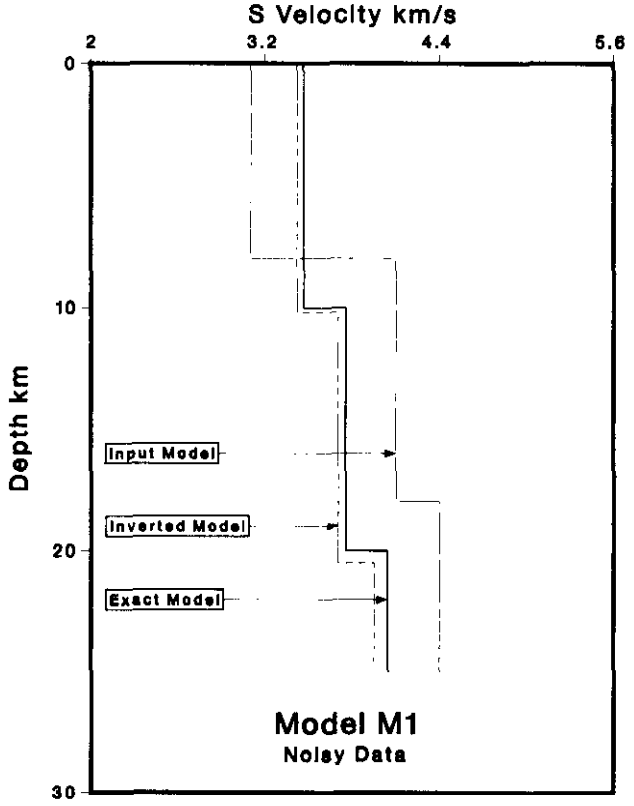

Fig. 7. Inverted shear-wave velocity model M1 obtained from the noisy amplitude data shown in Figure 6.

only may not be enough to pinpoint the difference. This is because the seismogram usually contains a lot of noise which tends to mask the actual arrivals in the record. Therefore, we suggest the application of the inversion algorithm in an attempt to resolve this problem. Even if the visual identification is extremely difficult, we may try different input models until we establish that no other solution is possible except the one with multiple arrivals. A trial and error process may be required, but many of the erroneous solutions may be eliminated using previous knowledge of the approximate structure and this approach. Apart from the usual nonuniqueness of the inverse problems, a solution based on the primary-arrival assumption is most unlikely to occur because the amplitude function depends on a number of factors such as velocity, depth, reflection coefficient and geometrical divergence of the wavefront, and only a specific combination of the contributing factors will determine its magnitude. Figure 10 shows the test data we have considered. Figure 11 and Table 4 include all the results obtained from the iterative inversion of contaminated multiple-reflection arrivals. Table 5 shows the result of an attempt to invert a set of noise-free multiple-reflection data in terms of an intentionally wrong assumption of primary arrivals. The program unsuccessfully attempts to find a local minimum around the approximate initial solution. As expected, the result is an absolute nonconvergence. Even after 100 iterations, the program fails to converge to a realistic model. The opposite situation, where primary reflections were assumed to be multiple reflections, also led to a divergent solution. We are, therefore, encouraged to conclude that the program is able to distinguish between multiple and primary reflections by leading to divergent solutions when an erroneous assumption is made about the nature of the particular phase on a reflection profile.

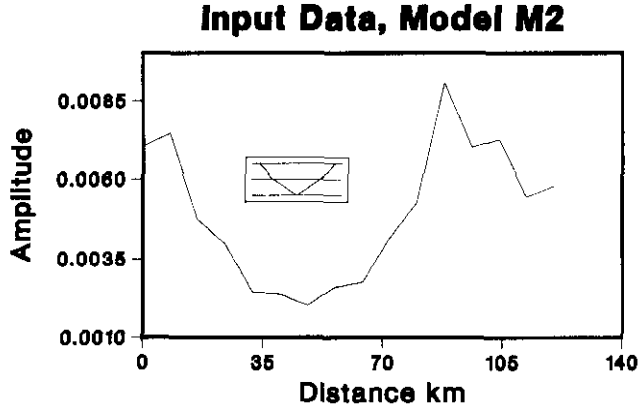

Fig. 8. Synthetic amplitude data for a 3-layer model M2 with low velocity in the middle crust.

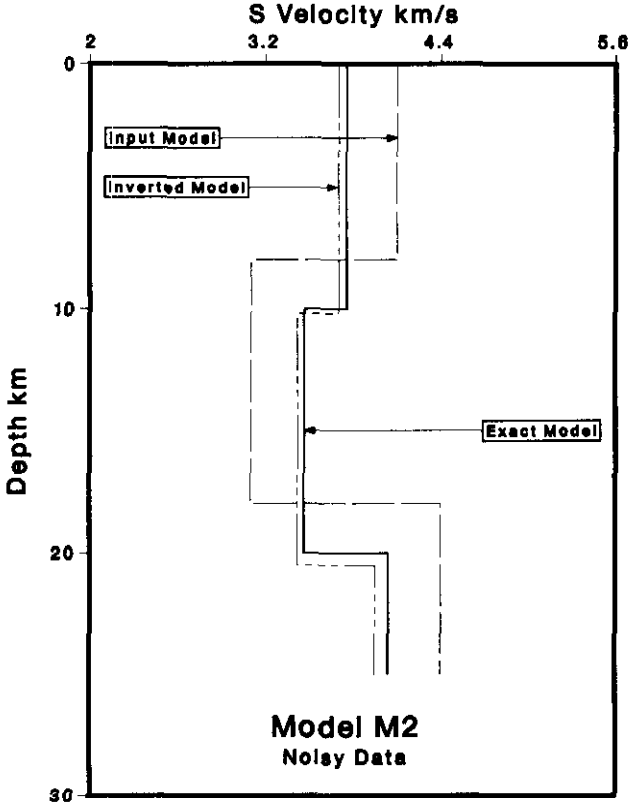

Fig. 9. Results of inversion of noisy amplitude data shown in Figure 8 for the low-velocity model M2.

Conclusion

We have shown that:

1) Parameterization of the forward model is convenient using Asymptotic Ray Theory. Useful parameters which contribute actively and effectively to the response function may be selected to reveal important physical properties of the medium under study.
2) Inversion of quantitative amplitude information is possible, which is a more rigorous and logical approach than visual waveform matching of synthetic seismograms to field data.
3) Amplitude information in the vertical component seismograms may be utilized to reveal additional information, such as shear-wave velocities and densities, without referring to the radial component seismograms.

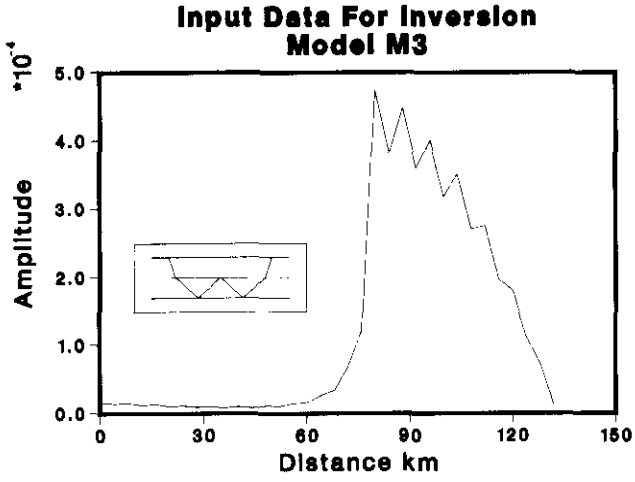

Fig. 10. Synthetic amplitude data for the velocity model M3 with multiple-reflection arrivals.

Layer	Exact model	Inverted Model	Resolution (diagonal)	Standard Deviation
	P-Velocity km/s			
1	6.0	6.036	1.00	.0323
2	6.5	6.550	1.00	.0510
3	7.0	7.045	1.00	.0432
	S-Velocity km/s			
1	3.464	3.500	1.00	.0457
2	3.753	3.807	1.00	.0561
3	4.042	3.993	1.00	.0282
	Density gm/cc			
1	2.525	2.531	1.00	.0234
2	2.714	2.742	1.00	.0346
3	2.904	2.856	1.00	.0584

Table 4. Results from iterative inversion of noisy multiple-reflection amplitude data.

Layer	Exact model	Inverted Model	Resolution (diagonal)	Standard Deviation
	P-Velocity km/s			
1	6.0	7.206	1.00	1.8500
2	6.5	8.495	1.00	2.1200
3	7.0	9.045	1.00	2.0130
	S-Velocity km/s			
1	3.464	4.371	1.00	1.5700
2	3.753	4.950	1.00	1.8640
3	4.042	5.885	1.00	1.8660
	Density gm/cc			
1	2.525	2.202	1.00	.43030
2	2.714	2.316	1.00	.54310
3	2.904	3.612	1.00	.67420

Table 5. Results from iterative inversion of multiple-reflection data with wrong primary arrival assumption.

4) The program is efficient in handling multiple-layer amplitude data, multiple shot points, multiple reflections and low-velocity zones.
5) Analytical calculations for the response function and its derivatives were preferred because of their accuracy and speed compared to numerical calculations.
6) Final testing of the method using field data is crucial. Therefore, future studies should attempt inversions using field amplitude data. It is also possible to design the inversion algorithm such that it will match both kinematic and dynamic data simultaneously. Such improvements may require special methods of matrix inversion (*e.g.*, the partition method). The potential benefits may make the more time-consuming and computationally more expensive method worthwhile.

REFERENCES

Aki, K. and Lee, W.H.K., 1976, Determination of three-dimensional velocity anomalies under a seismic array using first P arrival times from local earthquakes, 1. A Homogeneous initial model: J. Geophys. Res. **81**, 4381-4399.

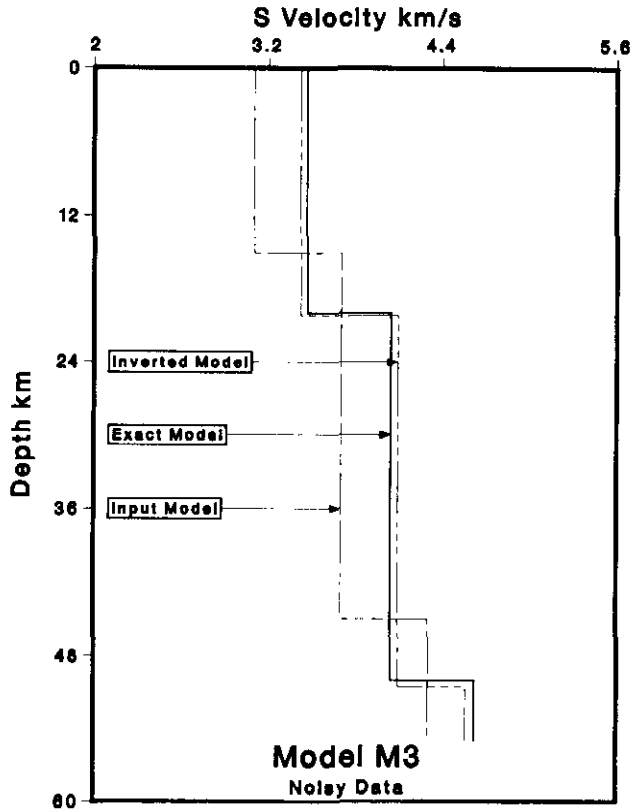

Fig. 11. Inverted velocity model M3 from noisy multiple-reflection amplitude data shown in Figure 10.

_____ and Richards, P., 1980, Quantitative seismology theory and methods, Vol 2: W.H. Freeman & Co., 522-540.
Benz, H.M. and Smith, R.B., 1984, Simultaneous inversion for lateral velocity variations and hypocenter in the Yellowstone region using earthquake and refraction data: J. Geophys. Res. **89**, 1208-1220.
Birch, F., 1964, Density and composition of mantle and core: J. Geophys. Res. **69**, 4377-4387.
Braile, L.W., 1973, Inversion of crustal seismic refraction and reflection data: J. Geophys. Res. **78**, 7738-7744.
Cerveny, V. and Ravindra, R., 1971, Theory of seismic head waves: Univ. of Toronto Press.
Chiu, S.K.L., Kanasewich, E.R. and Phadke, S., 1986, Three-dimensional determination of structure and velocity by seismic tomography: Geophysics **51**, 1559-1571.
Crosson, R.S., 1976, Crustal structure modeling of earthquake data. 1. Simultaneous least squares estimation of hypocenter and velocity parameters: J. Geophys. Res. **81**, 3036-3046.
Forsythe, G.E., Malcom, M.A. and Moler, C.B., 1977, Computer methods for mathematical computations: Prentice-Hall Inc., 227-235.
Golub, G.H. and Reinsch, C., 1970, Singular value decomposition and least squares solution: handbook for automatic computation, II, linear algebra, Eds., J. Wilkinson & C. Reinsch, Springer-Verlag New York, Inc.
Hirahara, K. and Ishikawa, Y., 1984, Travel time inversion for three-dimensional P-wave velocity anisotropy: J. Physics of the Earth **32**, 197-218.
Hoerl, A.E., Kennard, R.W. and Baldwin, K.F., 1975, Ridge regression: some simulations: Comm. Stat. **4**, 105-123.
Hoversten, G.M., Dey, A. and Morrison, H.F., 1982, Comparison of five least-squares inversion techniques in resistivity sounding: Geophys. Prosp. **30**, 688-715.
Ivansson, S., 1985, A study of methods for tomographic velocity estimation in the presence of low-velocity zones: Geophysics **50**, 969-988.
Lanczos, C., 1961, Linear differential operators: D. Van Nostrand Co., 665-679.
Lines, L.R. and Treitel, S., 1984, Tutorial — a review of least-squares inversion and its application to geophysical problems: Geophys. Prosp. **32**, 159-186.

Marks, L.W. and Hron, F., 1979, Dynamic properties of reflected and head waves near the critical point: Can. J. Earth Sciences **16**, 1388-1401.

Shahriar, M., Hron, F. and Cumming, G.L., 1987, Computer aided inversion of ray amplitudes and travel times by a linearized iterative method: Advances in Electronics and Electron Physics **51**, Academic Press Inc., in press.

Ursin, B. and Zheng, Y., 1985, Identification of seismic reflections using singular value decomposition: Geophys. Prosp. **33**, 773-799.

Vignersesse, J.L., 1978, Damped and constrained least squares method with application to gravity interpretation: J. Geophys. **45**, 17-28.